Polymer-Modified Mesoporous Silica Thin Films for Redox-Mediated Selective Membrane Gating

Johannes Elbert, Fabio Krohm, Christian Rüttiger, Sandra Kienle, Haiko Didzoleit, Bizan N. Balzer, Thorsten Hugel, Bernd Stühn, Markus Gallei, and Annette Brunsen**

Controlling structure and function to switch ionic transport through synthetic membranes is a major challenge in the fabrication of functional nanodevices. Here we describe the combination of mesoporous silica thin films as structural unit, functionalized with two different redox-responsive ferrocene-containing polymers, polyvinylferrocene (PVFc) and poly(2-(methacryloyloxy)ethyl ferrocenecarboxylate) (PFcMA), by using either a grafting to, or a grafting from approach. Both mesoporous film functionalization strategies are investigated in terms of polymer effect on ionic permselectivity. A significantly different ionic permselective behavior can be observed. This is attributed to different polymer location within the mesoporous film, depending on the functionalization strategies used. Additionally, the influence of chemical oxidation on the ionic permselective behavior is studied by cyclic voltammetry showing a redox-controlled membrane gating as function of polymer location and the pH value. This study is a first step of combining redox-responsive ferrocene-containing polymers and mesoporous membranes, and thus towards redox-controlled ionic transport through nanopores.

1. Introduction

Synthetic channels and transport control is of critical importance, for example, in separation and filtration application; and the use of hybrid mesoporous materials for such technological application is a broad and growing field.[1–5] Observing nature, transport through pores, for example, through ion channels, can be selective, gated, and directed. Their highly sophisticated channel function, originates from the interplay of their elaborate structure and functional organization on nanometer scale.[6,7]

J. Elbert, F. Krohm, C. Rüttiger, Dr. M. Gallei, Prof. A. Brunsen
Ernst-Berl Institut für Technische und Makromolekulare Chemie
Technische Universität Darmstadt
Petersenstraße 22, D-64287, Darmstadt, Germany
E-mail: m.gallei@mc.tu-darmstadt.de; brunsen@cellulose.tu-darmstadt.de
S. Kienle, B. N. Balzer, Prof. T. Hugel
IMETUM and Physik-Department
Technische Universität München
Boltzmannstr.11, D-85748, Garching, Germany
H. Didzoleit, Prof. B. Stühn
Institute of Condensed Matter Physics
Technische Universität Darmstadt
Hochschulstraße 8, D-64289, Darmstadt, Germany

DOI: 10.1002/adfm.201302304

The idea to create nanostructured hybrid systems that can function in a similar way as biological ion channels and pores emerged in the last decade.[8–14] So far, most explanations of ion conduction in synthetic pores have been based on the notion that an "open" and "closed" state of the channel exists, and that the transition between them results from physicochemical changes in the channel environment.[15] For example, in the case of ligand-activated ion channel gating, a ligand binds to receptor domains in the channel, inducing conformational changes that lead to opening of the ion conducting pore.

The combination of mesoporous films as structural unit and surface grafted responsive polymers as functional unit, is a versatile approach towards membranes with responsive surface properties such as surface charge, and consequently an approach towards adjustable ionic permselectivity for example.[16] With the correct choice of building blocks and self-assembly conditions, it is possible to produce nanostructured materials via sol–gel processes with precisely defined and tunable chemical functions incorporated into ordered mesostructured frameworks or postgrafted to the porewall after mesoporous film preparation and template removal.[17] Consecutively, the incorporation of polymer brushes[18–20] into the mesopores enables a precise control over the density of functional groups incorporated in the pores, as well as endows the mesoporous scaffold with built-in responses to chemical stimuli.[21] Thereby, the functionalization strategy such as grafting to by covalent or electrostatic binding,[22–24] or grafting from by using surface initiated polymerization protocols, might result in different functional density already on planar surfaces.[18,25–27] For mesoporous films, possible local differences due to limited diffusion might occur additionally.[8] The infiltration of polyelectrolytes into mesoporous silica, important for grafting to approaches, has been extensively explored by Caruso and collaborators, and subsequently exploited to build up mesoporous polymer-based spheres for delivery purposes.[28–31]

Concerning grafting from strategies for mesoporous matrices, only few surface-initiated polymerization techniques, mainly free radical, or controlled atom transfer radical polymerization (ATRP) are frequently used for grafting from polymerization in mesopores.[9,16,21,32,33] Although high grafting

densities allow access to stimuli-responsive polymer brushes for many important applications, the characterization of polymers obtained by this method is more challenging compared to the so-called grafting to approach.[18,25] In the latter case, end functionalized polymers can be used for immobilization leading to comparably low grafting densities.[34]

So far mainly polymers responsive to pH, or ionic strength for reversible change of surface properties, and thus ionic permselectivity, were investigated as internal trigger in mesoporous silica.[9,21,35–37] A further development is to look for external stimuli such as light.[8,38,39] Besides light as external trigger, applying a potential can result in a change of the oxidation levels maybe allowing similar switching rate.[40–42] To the best of our knowledge, ferrocene-containing polymers with the intrinsic capability to be reversibly stimulated by redox reagents and potential have not been applied for ion-selective gating in mesoporous silica membranes. While oxidizing the ferrocene moieties (electro)chemically, the polymer chains undergo a remarkable transition from hydrophobic to hydrophilic accompanied by an induction of charge.[40,43–46] The ferrocene oxidation/reduction cycles could be utilized for controlled release of organics from gels,[47] for applications as composite colloidal crystal films,[46] for responsive release of a dye from patchy nanocapsules,[48] for catalysis modulation,[49] or for switching surface wettability.[50]

Here, we report the functionalization of an ordered mesoporous silica thin film with redox-responsive poly(2-(methacryloyloxy)ethyl ferrocenecarboxylate) (PFcMA) and end functionalized polyvinylferrocene (PVFc). Therefore, PFcMA is immobilized by using a surface-initiated ATRP protocol, while end functionalized PVFc obtainable via living anionic polymerization is grafted to the surface of mesoporous silica. Both methods and polymers are compared in terms of functionalization and ionic permselectivity and a clear influence of the functionalization strategy on ionic permselectivity was observed. Due to ferrocene units as integral parts of the polymer chain, the redox state, and thus the charge of the polymer is varied and the redox-responsive ionic permselectivity is investigated by using cyclic voltammetry with charged, redox-active probe molecules. Samples are characterized by a combination of surface analytical tools such as IR-spectroscopy, ellipsometry, X-ray reflectometry, atomic force microscopy, and cyclic voltammetry.

2. Results and Discussion

2.1. Mesoporous Silica and Polymer Modification

Mesoporous silica films were obtained via one-pot sol-gel synthesis and evaporation induced self assembly[55,56] to silica and indium tin oxide (ITO) substrates using a sol containing tetraethoxysilane as the oxide precursor and nonionic block copolymer template Pluronic-F127 (for details see Experimental Section).[57] This experimental protocol led to 150–300-nm-thick mesoporous silica films featuring accessible mesopores

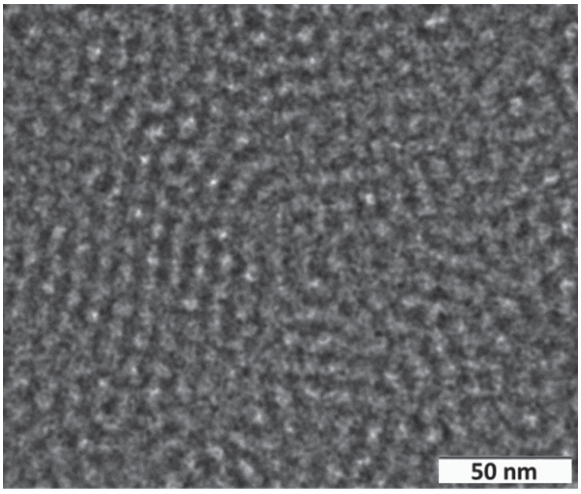

Figure 1. TEM image of a calcinated mesoporous silica film surface templated with Pluronic F127. The porous structure is clearly visible.

with a pore size in the range of 10 nm as derived from transmission electron microscopy (TEM) images (**Figure 1**).

This is in accordance with pore-ellipsometry of comparable films as published earlier.[24] Due to film shrinking the mesoporous film consists of elliptical pores with necks smaller than the pore diameter.[24] Film porosity was determined from ellipsometry data by using Brüggemann's effective medium approximation to be ≈45%. (**Table 1**).

Usually, for these systems porosity at 0% humidity is around 50%.[24] Differences in the porosity can be explained by changes in the humidity during the ellipsometric measurement. The humidity during ellipsometric measurements was not controlled but all samples of one series were measured under the same conditions, and hence can be compared with each other. Increasing humidity might lead to increased water adsorption and consequently to an increase in refractive index. A higher refractive index results in a lower porosity in the Brüggemann effective medium approximation. Thus, the porosity values summarized in Table 1 are rather slightly underestimated compared to the real porosity as further discussed below. Here, the deviation from earlier measurements at 0% humidity is below 10% in terms of porosity.[24]

The porosity and the presence of acid silanol groups at the silica walls, with a resulting pH-dependent charge, led to the development of negative surface charges on silica at pH > 3. This results, in general, into permselective properties of the mesoporous architecture, allowing selective transport or the

Table 1. Ellipsometry results for the mesoporous silica film, the initiator modified mesoporous silica film, and the PFcMA-containing mesoporous silica film, fitted with a one-layer model. Estimated porosity and pore filling based on the effective medium theory and refractive index values are summarized in the last column.

grafting from	refractive index	film thickness [nm]	pore filling
mesoporous silica	1.245	261	0% (porosity: 45%)
mesoporous silica + initiator	1.38	261	–
mesoporous silica + initiator + PFcMA	1.461	279	50%

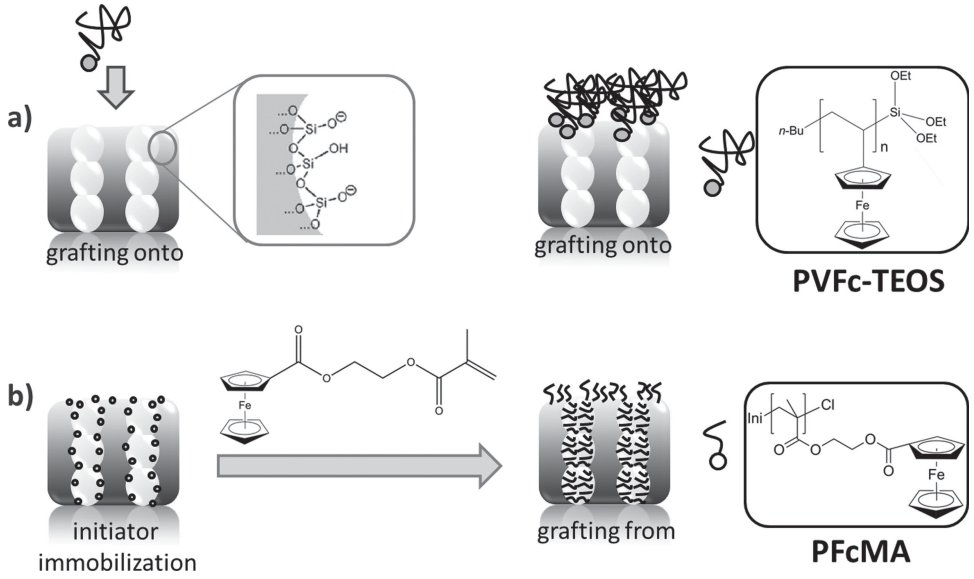

Figure 2. Overview on the mesoporous silica film functionalization strategies with redox responsive PVFc polymer by a) a grafting to approach and b) a grafting from approach of FcMA monomer by using SI-ATRP.

exclusion of ions.[58,59] To manipulate the permselective and the chemical properties by using external redox stimuli, we immobilized redox-responsive polymers to the mesoporous silica membrane by using two synthetic approaches (**Figure 2**): firstly, a grafting to procedure by using a PVFc carrying a triethoxysilane end group with a molecular weight of 2700 g mol^{-1} (M_w) for the PVFc precursor[49] was applied (Figure 2a). Secondly, we used a grafting from approach by using a surface initiated ATRP polymerization of FcMA monomer after immobilizing 3-(2-bromo*iso*butyrate)propyl trichlorosilane as initiator (Figure 2b). It has been previously reported that molar masses for surface-attached PFcMA and PFcMA chains obtained by ATRP in solution were in a comparable range.[51] All SEC results for the samples used are compiled in **Table 2**.

The presence of polymer in the PFcMA-modified mesoporous samples was monitored by infrared spectroscopy (**Figure 3**) and corroborated by XRR.

Figure 3 displays the measured IR spectra before and after a grafting from modification of the mesoporous silica thin film with PFcMA. The light grey empty circles shows a typical IR-spectrum of a pure mesoporous silica film, which displays the bands corresponding to the inorganic matrix: Si–OH and Si–O–Si stretching at ≈966 and ≈1070 cm^{-1}, respectively.[60] After polymer immobilization on the thin mesoporous silica film (grey filled circles and black filled triangles), these bands remained the same but the additional bands at ≈1727 cm^{-1} appeared. This signal was attributed to the presence of the C=O stretching of ester groups of the initiator (light grey empty circles) and the further signal increase to the PFcMA carbonyl group. A clear increase in the C=O ester vibrational signal at 1727 cm^{-1} is observed with prolonged polymerization time, as shown for a polymerization time of 12 min (grey filled circles) and 5 h (black triangles). Additionally,

Table 2. Comparison of molar masses of surface-attached end functionalized poly(vinylferrocene) (PVFc) and poly(2-(methacryloyloxy)ethyl ferrocenecarboxylate) (PFcMA) samples which were used in this study.

Sample	M_w[a)] [g mol^{-1}[	M_w[b)] [g mol^{-1}]	Reaction Time SI-ATRP
PVFc[b,c)]	1300	2700	—
PFcMA-1[d)]	4700	7500	12 min
PFcMA-2[d)]	14 300	32 900	5 h

[a)]Molecular weight obtained by SEC measurements vs PS standards; [b)]Molecular weight obtained by SEC-MALLS measurements, the refractive index increment dn/dc could be determined to 0.168 for PFcMA and 0.186 for PVFc; [c)]molar mass corresponds to PVFc precursor without TEOS functionality; [d)]Molar masses of PFcMA samples formed in solution ATRP.

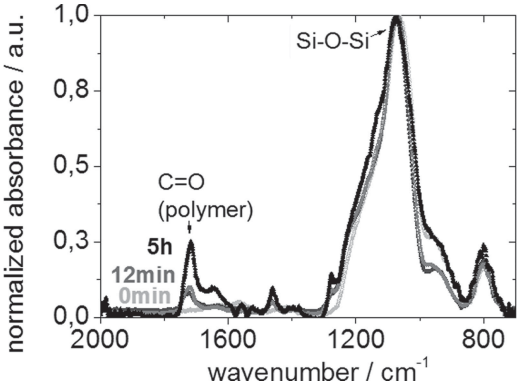

Figure 3. IR spectra of PFcMA-modified mesoporous silica thin films by using a grafting from protocol with increasing polymerization time of FcMA monomer. The unmodified mesoporous silica film (light grey empty circles) does not show a C=O signal at 1728 cm^{-1}, whereas the C=O signal increases form 12 min of polymerization (grey filled circles) to 5 h of polymerization (black filled triangles). Oxidation with $FeCl_3$ does not lead to a decrease in C=O signal (middle grey, for PFcMA sample after 12 min).

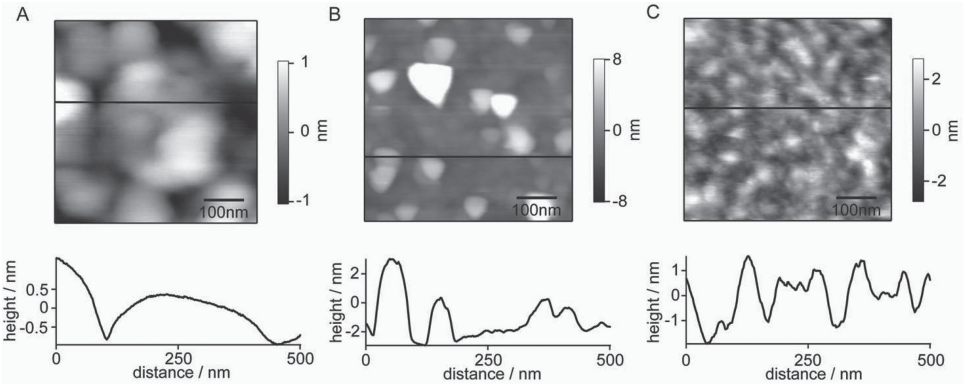

Figure 4. Characterization of the outer film surface by AFM after oxidation in aqueous KCl 100 mM to measure under identical conditions as compared to cyclic voltammetry. A) The mesoporous silica film as reference is shown in comparison to B) an oxidized PVFc-grafting to, and an C) oxidized PFcMA-grafting from-modified mesoporous silica thin film. The average values for the root mean square (RMS) roughness are shown in Figure S1, Supporting Information.

the signal for the 12 min sample (M_w = 7 500 g mol^{-1}) was recorded again after oxidation of the corresponding PFcMA sample, revealing no significant change of the IR spectrum. This indicates the stability of the PFcMA-functionalized mesoporous silica film under applied oxidation conditions. The PVFc-grafted thin mesoporous silica films cannot clearly be analyzed by IR-spectroscopy. The PVFc polymer does not carry a clearly indicating IR-active functional group such as a C=O bond. Thus, only the alkyl C–H stretching signal between 2850 and 2960 cm^{-1} can be used as an indication (Supporting Information, Figure S2), as well indicating the presence of polymer after grafting to of PVFc. Further surface characterization after oxidation and cyclic voltammetry measurements was carried out by AFM imaging (**Figure 4**).

AFM imaging of the outer PVFc- (Figure 4B) and PFcMA-modified (Figure 4C) mesoporous surface in 100 mM KCl solution (identical conditions compared to cyclic voltammetry experiments discussed below) indicated a polymer modification, based on the increase in roughness between the unmodified reference mesoporous silica film (Figure 4A), and the PVFc- (Figure 4B), and the PFcMA-modified (Figure 4C) mesoporous film. Because these images were obtained after oxidation and cyclic voltammetry measurements, they also show the stability of the polymer-modified mesoporous films under the applied experimental conditions. Additionally, a higher roughness was observed after grafting to of PVFc compared to samples modified with immobilized PFcMA by the grafting from approach indicating a more homogeneous distribution by using the latter approach. This is consistent with prior results obtained on planar surfaces.[50] An overview about the change in roughness on the scale of 500 nm × 500 nm measured in dry state, as well as in 100 mM KCl is given in the Supporting Information (Figure S1).

In **Figure 5**a we display the X-ray reflectivity results obtained from the mesoporous silica film (top, black), the film modified

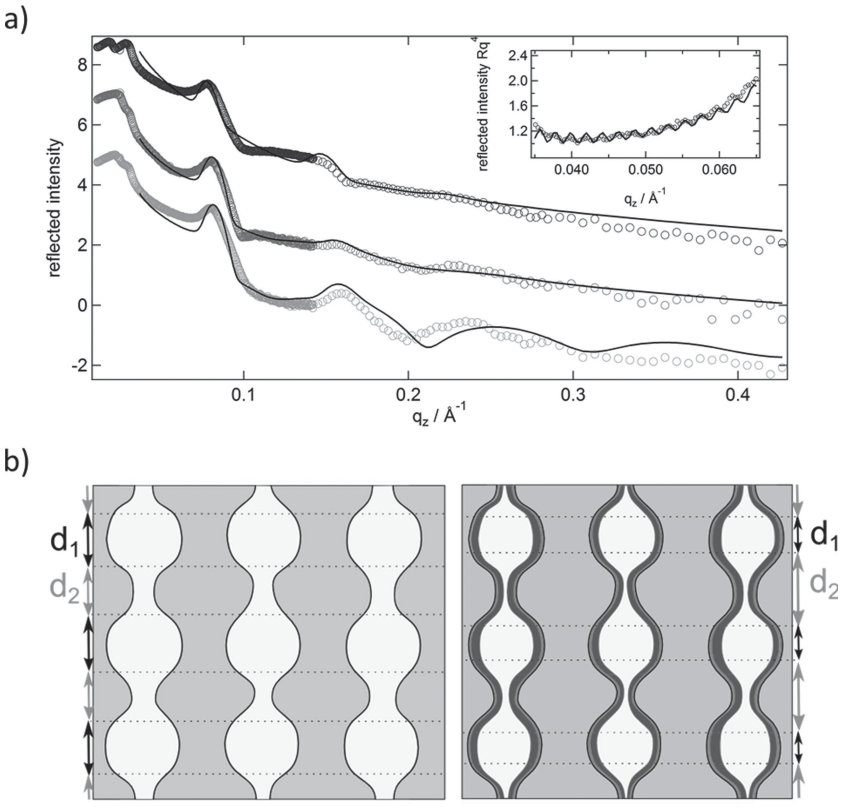

Figure 5. a) Reflected intensities from mesoporous silica (top, black), added initiator (middle, grey), added initiator and PFcMA (bottom, light grey). Curves are shifted for clarity of presentation. Full lines are fits with model as described in the text. The insert shows Kiessig fringes that allow to estimate total film thickness. b) Schematic arrangement of pores as derived from the internal film structure in XRR. Left: mesoporous silica: Interconnected pores with roughly equal thickness of sublayers. Right: modified pores. Sublayers of different thickness.

with initiator (middle, grey), and the film with PFcMA (bottom, light grey).

The reflectivity of the mesoporous silica film shows one strong peak on the background of the overall intensity decay. Closer inspection of the data in the insert of Figure 5a reveals weak Kiessig fringes which are the result of the interference of reflection from the lower and upper plane of the film. They allow to estimate a film thickness of 283 nm in good accordance with the result from ellipsometry. The position of the Bragg peak is at $q_z = 0.0785$ Å^{-1}. This corresponds to a periodicity of $d \approx 8.0$ nm. The mesoporous film therefore consists of approximately 35 layers with a thickness of 8 nm each. Such a multilayer should show higher order reflections which obviously are not present in our data. The absence in particular of the second order reflection is an indication for a substructure of the layers leading to the extinction of the intensity. We are therefore led to introduce 2 sublayers. A fit using this multilayer model is shown in the Figure 5b. It obviously captures the main form of the curve but deviates in details. We were unable to obtain a better fit which may be due to a heterogeneous structure in the film maybe due to inhomogeneous polymer distribution. The result is a sublayer of 4 nm with an electron density of 505 e nm^{-3} and a second sublayer of 4.8 nm and density 560 e nm^{-3} (Supporting Information, Table S1). These layers may be the result of pores organized in layers with connecting channels through a silica wall in a second layer as schematically depicted in Figure 5b. The lateral average then results in the experimentally determined density $\rho(z)$. Turning to the modified film (red curve) and finally to the film grafted with PFcMA the most striking difference is the appearance of higher order maxima of the Bragg peak. There is no strong shift in the position of the first peak. This clearly indicates a change in the internal structure of the layers with no change in the overall structure. The pores have at least partly been filled and the variation of electron density ρ(z) has been modified. A fit of these data with the multilayer model is indeed possible and included in Figure 5a as the full lines. These fits include a top layer of TEOS-initiator, and two layers of TEOS-Initiator and PFcMA, respectively. Parameters describing the structure of the multilayer are compiled in the Supporting Information (Table S1).

The presence of polymer within the porous membrane should lead to a change in optical properties and an increase in the refractive index. Ellipsometry measurements at ambient conditions indicated an increase in refractive index upon initiator binding and a further increase in refractive index upon polymer grafting from modification (Table 1). The obtained thickness increases upon PFcMA grafting from. But absolute values have to be taken with care due to inhomogeneities in film thickness along the substrate, especially in case of small substrates, due to the silica film preparation process. Variation in the range of 30% for these substrates can occur. Based on the effective medium theory (details in experimental section), the porosity, corresponding to the ratio of air within the film volume, and the pore filling can be estimated. Thereby, one has to be aware that these measurements were performed under ambient conditions and not at 0% humidity, which might influence the absolute values as discussed above. Based on adsorption isotherms of comparable mesoporous silica thin films water adsorption is low until a partial pressure of around 50%.[24] Measurements were carried out at humidity values below 40% and thus the error within the absolute values should allow a comparison of different functionalization states. Polymerization of PFcMA led to a pore filling in the range of 50% which means that 50% of the pore volume is occupied by polymer. This can be expected for a successful polymerization and even larger pore fillings were reported in the literature so far for radical polymerization in pores.[33,61] Furthermore, root mean square error (RMSE) values, indicating the quality of the fitting, are in an acceptable range indicating the presence of polymer in the entire film in case of PFcMA modification as corroborated by XRR (Figure 5). Compared to the results obtained for the mesoporous silica with immobilized PFcMA, the characterization of the PVFc-modified samples by using ellipsometry was difficult due to high RMSE values in the fitting process. Only a weak indication for an inhomogeneous polymer distribution along the mesoporous film can be given. Due to this the ellipsometry results after PVFc modification are not further discussed here.

Table 3. Contact angle of the outer film surface before and after PVFc-functionalization and before and after oxidation. Exemplified pictures are presented in Supporting Information, Figure S3.

	unmodified mesoporous silica [°]	reduced [°]	oxidized [°]
PVFc	19 (±7)	86 (±2)	75 (±2)
PFcMA-1 (12 min)	19 (±7)	75 (±3)	67 (±3)
PFcMA-2 (5 h)	19 (± 7)	83 (±2)	60 (±5)

Polymer modification as well as a change in oxidation state is expected to result in a change of surface properties, and especially in a change in hydrophobicity. Mesoporous silica thin films are hydrophilic and water enters the pores rapidly resulting in a low static contact angle, usually between 10° and 20° (**Table 3**). PFcMA and especially PVFc polymers are more hydrophobic and polymer modification is expected to lead to an increasing static contact angle of the outer film surface. Ferrocene-containing polymer layers grafted on a planar wafer substrate resulted in contact angles up to 104° depending on the grafting strategy, the polymer backbone, and the molecular weight of the polymer as shown earlier.[50] For the modification of mesoporous silica thin films a contact angle of approximately 86° for the grafting to strategy and a contact angle in the range of 75° and 83° in case of grafting from modification (PFcMA) with a short polymerization time (12 min, **PFcMA-1**) and a longer polymerization time of 5 h (**PFcMA-2**) were observed. The exact values are summarized in Table 3 and respective contact angle images are shown in the Supporting Information (Figure S3).

Oxidation of the polymer ferrocene units (**Figure 6**) results in a more hydrophilic polymer as compared to the reduced state, and thus a decrease in static contact angle is observed. Thereby the contact angle change is larger for the PFcMA compared to the PVFc modified mesoporous silica film and increases with increasing polymerization time which is in agreement with results obtained for planar surfaces as published earlier.[50]

The observed reduction in contact angle by oxidation was in the range of 10° for the grafting to and grafting from in case

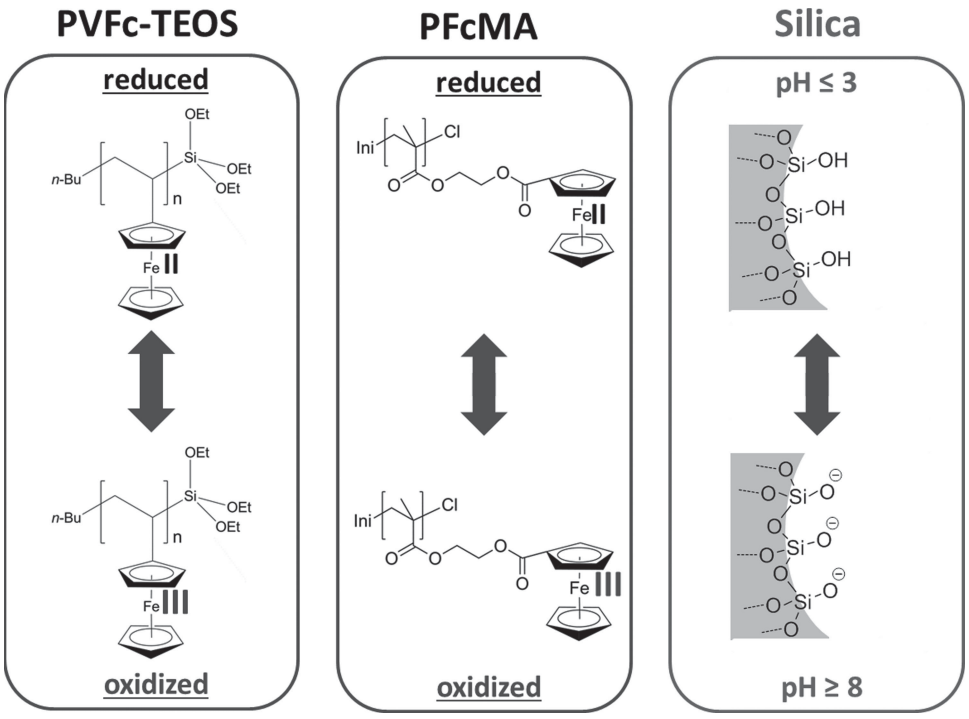

Figure 6. Charges relevant for surface energy and ionic permselectivity. Depending on the redox state the PVFc and PFcMA polymers are either neutral (reduced-) or positively charged (oxidized state). Depending on the pH the silica walls are either neutral (pH ≤ 3) or negatively charged (pH ≥ 8).

of a short polymerization time and in the range of 20° in case of the grafted from PFcMA with a long polymerization time of 5 h. The magnitude of contact angle decrease upon oxidation thereby depends among other parameters on the oxidation reagent as shown in a prior publication.[50] Therefore, all oxidations were carried out with $FeCl_3$ under identical conditions.

2.2. Ionic Transport: Grafting to

The ionic permselective properties of the mesostructured redox-responsive polymer modified hybrid interface were electrochemically probed using molecular anionic and cationic redox probes, $Fe(CN_6)^{3-}$ and $Ru(NH_3)_6^{3+}$, respectively. These probe molecules can diffuse across the mesoporous film deposited on a conductive ITO substrate to be detected at the ITO substrate electrode.[53,58] Thereby, mesoporous films modified in a grafting to approach (**Figure 7**), or modified in a grafting from approach (as discussed below) resulted in significantly different permselectivity behavior. Figure 7b,c display exemplified cyclic voltammograms of a mesoporous film with PVFc polymer functionalized in a grafting to approach compared to an unmodified mesoporous silica film (Figure 7a).

In the case of bare mesoporous silica films (Figure 7a), and a basic pH ≥ 8, a well-defined, strong electrochemical response of $Ru(NH_3)_6^{3+}$ (redoxpotential between –0.6 and +0.2 V, red) ions was observed whereas similar experiments performed in the presence of $Fe(CN_6)^{3-}$ (redox potential between –0.2 and +0.6 V) revealed that the electron transfer at the underlying ITO interface was strongly hindered (red, Figure 7a). This can be ascribed to the fact that the negatively charged pore walls at pH ≥ 8 exclude the anionic probes from the inner surroundings of the inorganic film due to a Debeye screening length being in the range of the neck size. The enhanced electrochemical response, as compared to the cyclic voltammogram of the bare ITO electrode in the presence of the cationic redox probe solution (Figure 7b,c, light grey dashed trace), reflects the fact that the silica mesoporous film is able to preconcentrate $Ru(NH_3)_6^{3+}$ species in the inner environment of the 3D pore array. In this scenario, the attractive electrostatic interactions in the mesopore environment are the main driving force, leading to the preconcentration of the cationic probe within the porous framework. This observation is in agreement with earlier studies performed on comparable mesoporous systems.[24,62,63] Switching the pH to more acidic environment pH ≤ 3, the silica pore walls are neutralized and electrostatic interactions are "switched off". This is again reflected in the cyclic voltammograms showing a peak current comparable for both cationic and anionic probe molecules, which is as well comparable to a bare ITO signal, reflecting unhindered diffusion through the entire mesoporous film until the electrode interface. Within this discussion it has to be taken into account that mentioned pH-values always refer to the solution pH and that pH-values within the mesopores might be significantly different in dependence of confinement, surface functionality, and curvature, which is not further discussed here.[64,65]

After modification of the mesoporous silica film with redox-responsive polymer PVFc in a grafting to approach, this ionic permselective behavior changes as demonstrated in Figure 7b. In case of a reduced and thus neutral polymer and a neutral mesoporous silica wall (pH ≤ 3) (Figure 7b, filled triangles) the diffusion of both probe molecules is strongly hindered up

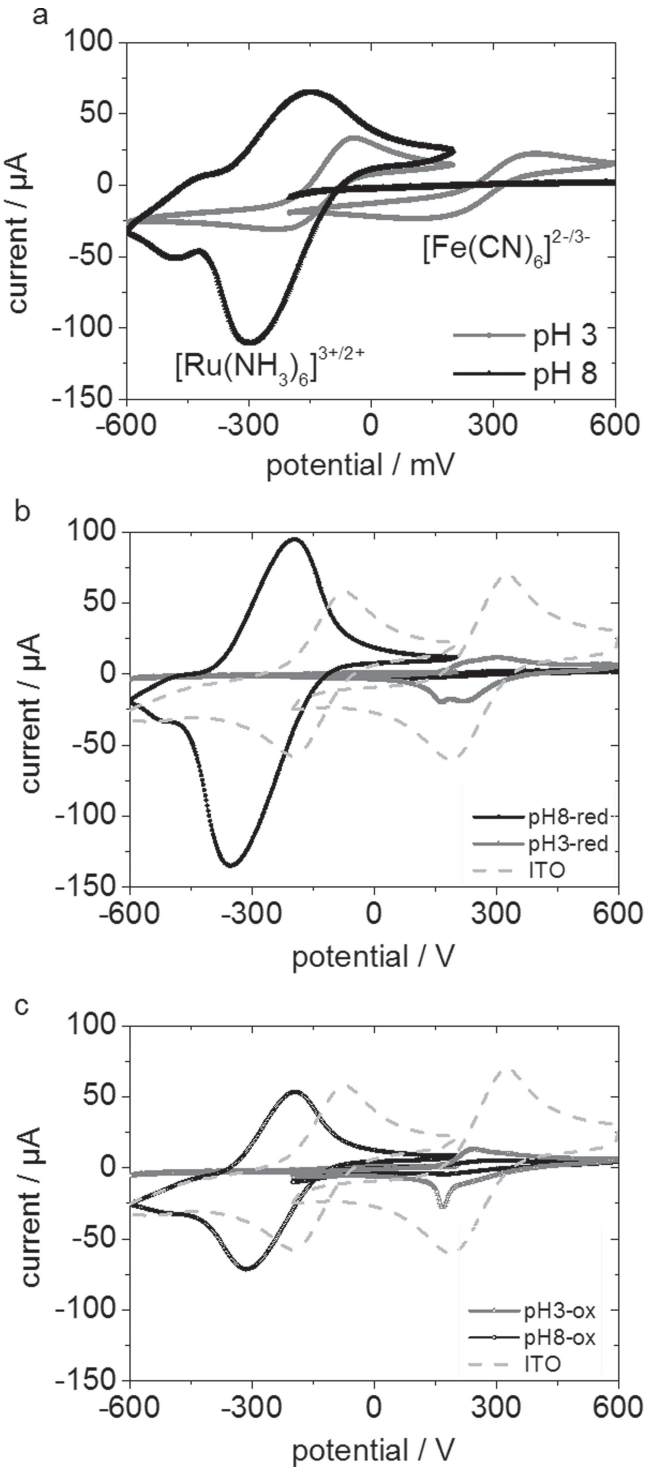

Figure 7. Exemplified cyclic voltammograms for an unmodified mesoporous silica thin film (a), and a PVFc-grafted to mesoporous silica film b) before, and c) after oxidation at pH 3 (grey line, grey triangles), and pH 8 (black line, black circles). For the PVFc-modified mesoporous films, b) the reduced state (filled symbols) and c) the oxidized state (empty symbols) is measured in dependence of pH. The probe solution was measured on the unmodified ITO electrode. The corresponding measurement is shown in light grey dashed lines.

to no probe molecule detection within the detection limit of our experiment, independent of its charge. Between different samples always a strong hindrance for both probe molecules under these conditions was observed. Small variation in peak-current (Ip) between no signal and a small signal as observed here for $Fe(CN_6)^{3-}$ were attributed to local inhomogeneities in polymer functionalization. A grafting to approach, in general, leads to much less dense polymer layers due to steric hindrance.[18] Changing solution pH to pH ≥ 8, and thus generating negatively charged mesoporous silica walls, leads to electrostatic exclusion of the negatively charged probe (Figure 7b, filled circles), as observed for unmodified mesoporous silica as well. In contrast to the polymer effect in an acidic environment, here the cationic probe reaches the electrode and shows a strong electrochemical signal indicating its preconcentration within the mesoporous silica film as observed for polymer free mesoporous silica. This observations indicates that the polymer layer seems to be predominantly located on the film solution interface of the mesoporous film and thus does not neutralize and reduce the pore wall charge of the mesoporous silica close to the electrode interface. This might be explained taking into account a thin polymer layer, not exceeding the debeye screening length, with a lower amount of charges as compared to the silica surface, and a thickness in the range of the debeye length. This is in accordance as well with the ellipsometry measurements which did not allow a clear fitting of data with a one-layer model as discussed above. The reduced polymer grafted to the mesoporous silica membrane results in strongly hindered diffusion of charged redox probes up to complete exclusion, as long as no electrostatic interaction between mesoporous silica walls and redox probes is induced by respective pH conditions. We attribute this "diffusion barrier effect" to the hydrophobicity of the PVFc layer (Table 3) with contact angles in the range of 84–88° for the reduced PVFc and still around 75° after oxidation. For hydrophobic nanopores, especially for carbon nanotubes, it is well known that a critical infiltration pressure, which scales with cos θ and the pore size, has to be overcome to infiltrate these pores with water.[66,67] In case of electrostatic attraction between the silica pore walls and the redox probe (pH ≥ 8, $Ru(NH_3)_6^{3+}$), the redox probe seems to be able to cross the polymer layer, and to reach the electrode, resulting a strongly increased Ip indicating preconcentration within the mesoporous film, comparable to unmodified mesoporous silica. The debeye screening length in a 100 mM KCl solution is around 1 nm. Thus a polymer layer thickness around this value as measured here and as observed for planar substrates[50] seems not to be able to completely screen electrostatic interaction of an underlying surface. Oxidizing the ferrocene moieties in PVFc, and thus introducing positive charges into the polymer layer, should lead to electrostatic repulsion between the polymer and the cationic $Ru(NH_3)_6^{3+}$ probe, as well as electrostatic attraction between the polymer and the anionic $Fe(CN_6)^{3-}$ probe. Detecting the probe diffusion by cyclic voltammetry only a significant change in the $Ru(NH_3)_6^{3+}$ response at pH ≤ 3 is observed (Figure 7c, black empty circles; Supporting Information, Figure S5). The detected Ip is reduced compared to the same conditions and a reduced and thus neutral polymer. This means the expected electrostatic attraction

between the anionic probe and the oxidized polymer does not lead to enhanced diffusion through the polymer layer until the electrode interface at the bottom of the mesoporous film. This points to the influence of eventual mechanical pore blocking, and wetting effects (contact angle 75°, Table 3) on probe molecule diffusion into the mesoporous membrane, which cannot be discriminated from electrostatic effects in the mesoporous film located below the polymer layer in the transport detection. The small additional peak in the $Fe(CN_6)^{3-}$ response (Figure 7c, grey empty triangles) is most probably due to Prussian blue formation as described in the literature,[68] and as observed for polymer grafted to the unmodified ITO electrode (Figure S4, Supporting Information).

Consequently, a grafted to polymer modification resulted into a polymer predominantly located at the solution membrane interface leading to hindered diffusion of charged redox probes. Nevertheless, this polymer layer was not able to shield electrostatic interaction between the bottom mesoporous silica membrane and the probe molecules, indicating a thickness smaller than the Debye screening length and a low density polymer layer due to the grafting to approach. Oxidation of the polymer led to a reduction in Ip in case of expected repulsive interaction between polymer and probe molecule by remaining attractive electrostatic interaction between the bottom silica membrane and the probe molecule but as well in this conformation the interaction between the bottom silica membrane and the probe molecules in solution could not be shielded completely.

2.3. Ionic Transport: Grafting from

Modification of a mesoporous silica membrane with the PFcMA redox responsive polymer in a grafting from approach along the entire film thickness, as well as on the outer surface results in a strong hindrance of accessibility already after initiator binding. **Figure 8** summarized the cyclic voltammograms for a cationic $Ru(NH_3)_6^{3+}$ probe and the anionic $Fe(CN_6)^{3-}$ probe at pH ≤ 3 and pH ≥ 8 in grey triangles and black circles, respectively. The corresponding scanrate dependent data can be found in the Supporting Information (Figure S6). The general behavior in dependence of pH can be compared to pure mesoporous silica showing a larger signal for the anionic probe at pH ≤ 3 were the silica pore walls are expected to be neutral. But compared to unmodified silica (Figure 7a) the signal is an order of magnitude smaller and thus the difference for the anionic probe between pH ≤ 3 and pH ≥ 8 is reduced. The same reduction of approximately one order of magnitude is observed for the cationic probe, whereas the difference between acidic and basic pH are larger showing the electrostatic attraction between the negatively charged silanol groups at the pore wall and the cationic probe molecule at pH ≥ 8 (Figure 8, black circles). Post-grafting of initiator molecules leads to a filling of pores and to an increase in hydrophobicity with a static contact angle on the outer mesoporous film surface around 70°. Thus wetting might be a determining parameter responsible for the overall reduction in detected current. As mentioned above contact angle and pore size are decisive for water infiltration in pores with nanometer size,[66,67] and in inverse opal films this concept was even used to pattern wetting profiles.[69]

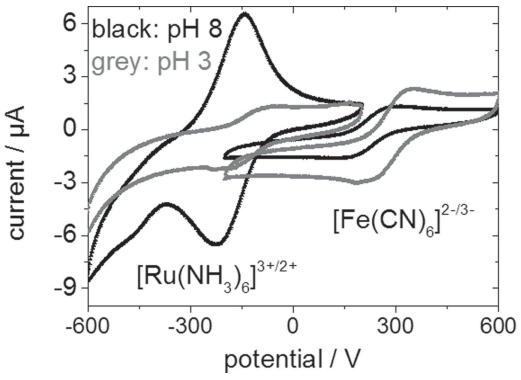

Figure 8. Cyclic voltammograms for initiator modified pore surface at pH 3 (grey triangles) and pH 8 (black circles) for a positively $(Ru(NH_3)_6^{3+}$, –0.6 to 0.2 V) and negatively charged $(Fe(CN_6)^{3-}$, –0.2 to 0.6 V) probe molecule in 100 mM KCl at a scanrate of 200 mV s^{-1}.

After PFcMA modification by using the grafting from approach permselectivity was again characterized by using charged redox probe molecules. The cyclic voltammograms for the reduced polymer are shown in **Figure 9**a and the results after polymer oxidation in Figure 9b. Grafting from of PFcMA polymer led to even further decrease in mass transport and thus decrease in detected current density. For the anionic probe molecules pores are almost not accessible anymore

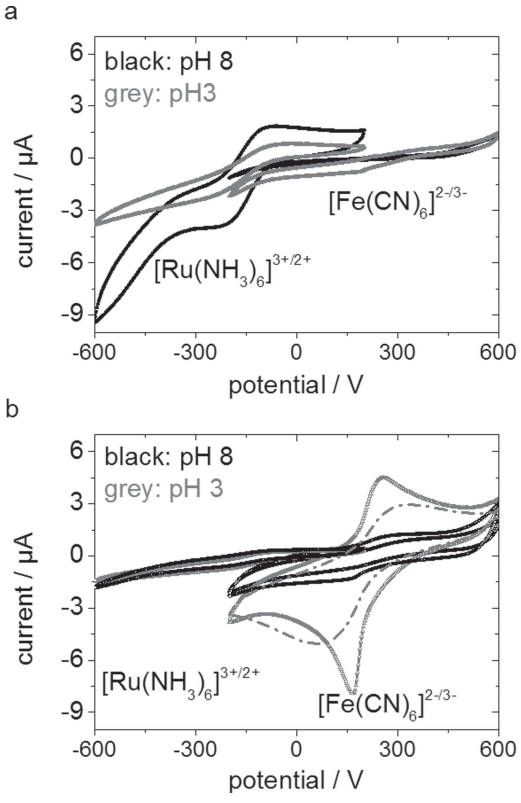

Figure 9. Cyclic voltammograms for a) reduced (filled symbols) and b) oxidized (empty symbols) at pH 3 (grey triangles) and pH 8 (black circles) for a positively $(Ru(NH_3)_6^{3+}$, –0.6 to 0.2 V) and negatively charged $(Fe(CN_6)^{3-}$, –0.2 to 0.6 V) probe molecule in 100 mM KCl at a scanrate of 200 mV s^{-1}.

and pH changes do not show a major effect. The mesoporous films show a slightly higher accessibility for the cationic probe, especially at basic pH whereas nevertheless no preconcentration can be observed indicating a complete shielding of the pore wall charge due to polymer filling of pores and maybe as well due to increasing hydrophobicity upon polymer functionalization.

Although the overall detected current is very small, oxidation of the grafted from PFcMA polymer results in a change of permselective properties: The signal for the cationic $Ru(NH_3)_6^{3+}$ probe molecule (Figure 9b) dropped to basically zero, independent of pH indicating an additional electrostatic repulsion as expected due to positively charged ferrocene units within the polymer after oxidation. In contrast to this observation the response for the negatively charged $Fe(CN_6)^{3-}$ probe molecules was still dependent on pH and showed a signal increase at pH ≤ 3 indicating first an electrostatic attraction between the oxidized polymer and the negatively charged probe molecule, although the overall current remained very small with $\approx 3 \times 10^{-6}$ µA. Thereby the sharp dip in one of the cyclic voltammograms in Figure 9b is most probably correlated with Prussian blue formation as described in the literature,[68] and visible by observing a blue colour on the electrode after the measurement. This peak shape was observed for a pure oxidized polymer layer directly deposited onto a planar ITO surface for the $Fe(CN_6)^{3-}$ probe at an acidic pH as well (Supporting Information, Figure S4b), and could be reduced by intensive incubation in supporting electrolyte solution for several hours in case of the mesoporous polymer modified membrane (Figure 9b, grey dashed trace). The effect that basic pH reduces this response almost to zero (Figure 9b, red $Fe(CN_6)^{3-}$) might be correlated to incomplete oxidation not compensating the entire amount of charges at the silica pore wall, and to the influence of hydrophobicity and pore filling.

3. Conclusion

In summary, we showed the synthetic modification of mesoporous silica films with redox-responsive ferrocene-containing polymers by a grafting to and a grafting from approach. The grafting to approach rather led to a polymer layer predominantly located on the mesoporous film solution interface, whereas the grafting from approach resulted into polymer modification along the entire film thickness. Depending on the synthetic approach the permselective behavior was significantly different. Grafting to of a PVFc polymer layer mostly located at the outer film surface resulted in a diffusion barrier which was attributed due to a hydrophobic outer surface. This diffusion barrier was not able to shield electrostatic interaction with bottom mesoporous silica film, and could be crossed by ions in case of attractive electrostatic interaction with the subjacent mesoporous silica layer. After grafting from of a PFcMA polymer the increasing hydrophobicity and pore filling resulted in a significant decrease of detected current but the electrostatic effect of oxidizing the ferrocene units was clearly visible in an increase of detected current in the absence of charged silanol groups. Nevertheless, a pH effect still visible for the oxidized PFcMA indicates a relatively low amount of oxidized ferrocene units, which cannot completely compensate the mesoporous silica wall charges at a basic pH. All these results point towards the importance of polymer functionalization strategies to manipulate ionic permselectivity in mesoporous membranes, and advance a fascinating field of redox gating of ionic transport in synthetic polymer-hybrid systems.

4. Experimental Section

Reagents: All chemicals and solvents were purchased from Fisher Scientific, Sigma-Aldrich and Alfa Aesar and used as received if not otherwise mentioned. Cu(I)Cl was washed five times with glacial acetic acid and ethanol. *N*-,*N*-,*N*′-,*N*′-,*N*″-Pentamethyldiethylenetriamine (PMDETA), anisole and *2*-bromo-*iso*-butyric *tert*-butylester (*t*BbiB) were degassed and stored under an argon atmosphere or in a glovebox. All ATRP were conducted under nitrogen or argon atmosphere. The copper complexes were freshly prepared in anisole and treated in the glovebox. Ferrocene was recrystallized from *n*-hexane. 2-(methacryloyloxy)ethyl ferrocenecarboxylate (FcMA) monomer **1** was synthesized described elsewhere.[51] Triethoxy functionalized polyvinylferrocenes (PVFc-TEOS) were synthesized via anionic polymerization as recently reported.[49]

Instrumentation: Standard SEC was performed with tetrahydrofuran (THF) as the mobile phase (flow rate 1 mL min^{-1}) on a SDV column set from PSS (SDV 1000, SDV 100000, SDV 1000000) at 30 °C. Calibration was carried out using PS standards (from Polymer Standard Service, Mainz). For the SEC-MALLS experiments, a system composed of a Waters 515 pump (Waters, Milford, CT), a TSP AS100 autosampler, a Waters column oven, a Waters 486 UV detector operating at 254 nm, a Waters 410 RI-detector, and a DAWN DSP light scattering detector (Wyatt Technology, Santa Barbara, CA) was used. For data acquisition and evaluation of the light-scattering experiments, Astra version 4.73 (Wyatt Technology, Santa Barbara, CA) was used. The light-scattering instrument was calibrated using pure toluene, assuming a Rayleigh ratio of 9.78×10^{-6} cm^{-1} at 690 nm. An injection volume of 118 µL, a sample concentration of 1–2 g L^{-1}, a column temperature of 35 °C, and a THF flow rate of 1 mL min^{-1} have been applied. SEC analysis was performed on a high resolution column set from PSS (SDV 5 µm 10^6 Å, SDV 5 µm 10^5 Å, SDV 5 µm 1000 Å).

Ellipsometry: The dry thickness of the surface attached films on silicon wafers was measured using a Nanofilm EP^3 imaging ellipsometer. One zone angle-of-incidence (AOI) variation measurements were captured between AOIs of 40° and 80° with a 658 nm laser in the centre of the substrate. The apparent film thickness was calculated from the measured angles Ψ and Δ, using the analysis software EP^4 supplied with the instrument. The fitting parameters for the silicon oxide layer thickness (t_{SiOx} = 2.0 nm, measured separately, prior to film immobilization) and the refractive index of the polymer layer ($n_{polymer}$ = 1.5) were kept constant. The mesoporous film or the polymer-modified mesoporous film was fitted with a one box model using one refractive index and one thickness value for data simulation. Porosity and pore filling were determined using the Brüggemann effective medium approximation as described elsewhere.[24,52]

Infrared Spectroscopy: IR spectroscopy measurements were performed on a Spectrum One (Perkin Elmer) instrument in attenuated total reflection (ATR) mode. Mesoporous film was scratched from the substrate to record IR spectra in a range from 4000 to 600 cm^{-1}. The measured spectra were background corrected and normalized to the Si-O-Si band at ≈1080 cm^{-1}.

Cyclic Voltammetry: Quantitative variations in permselectivity were studied by following the changes of voltammetric peak currents associated to cationic ($Ru(NH_3)_6^{2+/3+}$) and anionic ($Fe(CN)_6^{4-/3-}$) redox species diffusing across the mesoporous film.[53] As recently summarized by Walcarius,[54] changes in the voltammetric response of mesoporous electrodes reflect the changes in probe concentration or diffusion in response to external stimuli or the architecture of the pore. To this end, mesoporous films modified with redox-responsive polymer were

prepared on bare indium tin oxide (ITO) electrodes. The measurements were performed with a 2 mM solution of the probe molecule in a 100 mM solution of KCl as supporting electrolyte. pH was adjusted with NaOH or HCl. An Ag/AgCl electrode was used as reference electrode, and various scanrates between 10 mV s^{-1} and 1000 mV s^{-1} were measured. The measured electrode area was 0.21 cm^2.

Atomic Force Microscopy: The atomic force microscope imaging was performed in intermittent-contact mode with an MFP3D-SA (Asylum Research, USA). For measuring in air and in liquid (100 mM KCl) silicon cantilevers (AC240TS, Olympus, Japan) were used. The nominal spring constant is 2 N m^{-1} with a resonance frequency of 70 kHz in air. The scanrate was 0.5–1 Hz with a scan size of 500 nm × 500 nm. The root mean square (RMS) roughness was obtained with IgorPro (Wavemetrics) by averaging over the whole image.

X-Ray Reflectometry: X-ray reflectivity determines the intensity of the X-ray beam reflected from a planar surface. For an ideally flat surface of a bulk material one would receive an intensity that decays rapidly with increasing scattering angle according to Fresnel's formula. Deviations from this law are due to a variation of electron density along the surface normal and are used to determine the thickness and internal structure of thin films on a substrate. The reflected intensity at a scattering angle 2θ or the related scattering vector $q_z = 4\pi/\lambda \sin\theta$ may be calculated exactly on the basis of the electron density profile. In a good approximation at larger q it is given as (Born approximation):

$$I(q_z) \propto R_F \left| \int \frac{d\rho}{dz} e^{iq_z z} dz \right|^2 \quad (1)$$

Here, R_F denotes the Fresnel reflectivity which may be approximated as $R_F \propto 1/q_z^4$. The experiment therefore allows to determine the internal structure of thin films. The reflectometer is based on a D8 Advance diffractometer (Bruker AXS, Germany), which is designed to measure reflectivities in θ–θ geometry. X-ray source and detector were mounted on goniometer arms which can be moved independently with a precision of 0.001°. The X-ray beam was generated by a conventional X-ray tube with a Cu anode to yield CuK_α radiation with a wavelength of λ = 1.54 Å. The generated X-ray beam had a line focus and was monochromized by a Goebel mirror (W/Si multilayer mirror). Through a narrow slit of 0.1 mm the beam passed an absorber (calibrated Cu attenuator) which was used for high intensity near the critical angle in order to remain within the linear response regime of the detector. A second 0.1 mm slit was placed after the absorber to cut out the K_β-line (which is also reflected by the monochromator). Intensity was detected by a Vântec-1 line detector (Bruker AXS, Germany) providing the possibility to measure the specular reflected intensities and the diffuse reflected intensities simultaneously in an angular range of $\Delta\theta_f = 2°$ for a given incident angle θ_i. Within one measurement the detector collected intensity over all q_x (line focus). For each incident angle a single intensity $I(\theta_f)$ contained the specular and off-specular condition. The intensity of the reflected beam was determined as the integral of the specular peak corrected for background measured as the diffuse intensity. The specular reflectivities were analyzed using the Motofit Reflectometry package, rev. 409 for Igor Pro.

Synthesis of Mesoporous Silica Films: Mesoporous silica films were synthesized via a sol gel method based on the oxide precursor tetraethoxysilane (TEOS) in presence of the template (Pluronic F127). The precursor solution was prepared using the following molar ratios: 1 TEOS: 0.005 F127: 24 EtOH: 5.2 H_2O: 0.28 HCl. This solution was used to produce films by dip-coating on ITO, glass, or silicon wafer under 40–50% relative humidity at 298 K (2 mm s^{-1} withdrawing speed). Freshly deposited films were submitted to 50% relative humidity chamber for 1 h, followed by a stabilizing thermal treatment of two successive 1 hours steps at 60 °C and 130 °C, and a final 2 hours calcination at 350 °C with a temperature gradient of 1 °C min^{-1} between 130 °C and 350 °C. The films were cleaned by rinsing with ethanol.

Grafting PVFc-TEOS to Mesoporous Silica: The mesoporous silica films were placed in a Schlenk tube and dried in vacuo. The flask was refilled with argon prior to the addition of dry toluene (15 mL) and PVFc-TEOS (50 mg). The solution was heated to 120 °C for 24 h. The substrates were cleaned in a soxhlet apparatus with THF to remove physisorbed polymer.

Initiator Immobilization on Mesoporous Silica and SI-ATRP of FcMA: The mesoporous silica films were placed in a Schlenk tube and dried in vacuo. The flask was refilled with argon prior to the addition of dry toluene (20 mL) and 3-(2-bromo*iso*butyrate)propyl trichlorosilane (1 g, 2.92 mmol). After stirring at 60 °C for 16 h, the substrates were extracted with THF to remove physisorbed initiator. The initiator-functionalized mesoporous silica films were again placed in a Schlenk tube, dried in vacuo and the flask was refilled with argon. After the addition of anisole (25 mL), FcMA (2.5 g, 7.31 mmol) and 2-bromo*iso*butyric *tert*-butylester (10 µL, 0.05 mmol), the solution was heated to 90 °C for 10 min. The polymerization was initiated by adding a solution of [Cu^I(PMDETA)Cl] (0.2 M, 2 mL, 0.4 mmol in neat anisole). After 4 h of reaction time, the substrates were taken off the reaction vessel followed by soxhlet extraction with THF to remove physisorbed polymer. For characterization of PFcMA, which is formed in solution, aliquots were taken during the ATRP. These solutions were poured into a 10-fold excess of methanol. Precipitated polymers were filtered and dried in vacuo. PFcMA samples were characterized by using SEC-MALLS measurements.

Oxidation of Immobilized Ferrocene Polymers on Mesoporous Silica Films: The functionalized mesoporous silica films were placed in neat THF (10 mL) followed by the addition of $FeCl_3$ (0.31 mmol, 50 mg). After 16 h of stirring, the mesoporous silica film was extracted with THF and water followed by drying under ambient conditions for 12 h.

Supporting Information

Supporting Information is available from the Wiley Online Library or from the author. Additional data on X-ray reflectometry, atomic force microscopy, infrared spectroscopy for PVFc-modified mesoporous silica tin films, contact angle images, and cyclic voltammetry can be found in the Supporting Information.

Acknowledgements

The authors would like to thank the Landesoffensive zur Entwicklung Wissenschaftlich-ökonomischer Exzellenz (LOEWE "*Soft Control*") for financial support of this work. Annette Brunsen acknowledges the Robert Bosch Stiftung, the "Fonds der Chemischen Industrie" for funding, and Prof. Markus Biesalski for helpful support.

Received: July 9, 2013
Published online: November 20, 2013

[1] C. Sanchez, P. Belleville, M. Popall, L. Nicole, *Chem. Soc. Rev.* **2011**, *40*, 696.
[2] B. Lebeau, P. Innocenzi, *Chem. Soc. Rev.* **2011**, *40*, 886.
[3] C. Laberty-Robert, K. Valle, F. Pereira, C. Sanchez, *Chem. Soc. Rev.* **2011**, *40*, 961.
[4] E. Riccardi, J.-C. Wang, A. I. Liapis, *J. Phys. Chem. B* **2008**, *112*, 7478.
[5] I. Tan, F. Roohi, M.-M. Titirici, *Anal. Methods* **2012**, *4*, 34.
[6] H. Chung, O. S. Anderson, V. V. Krishnamurthy, Springer Verlag, Heidelberg **2010**.
[7] *Ion Channels: From Structure to Function* (Eds:J. Kew, C. Davies), Oxford University Press, Oxford **2010**.
[8] A. Brunsen, J. Cui, M. Ceolín, A. d. Campo, G. J. J. A. Soler-Illia, O. Azzaroni, *Chem. Commun.* **2012**, *48*, 1422.
[9] A. Brunsen, C. Diaz, L. I. Pietrasanta, B. Yameen, M. Ceolin, G. J. A. A. Soler-Illia, O. Azzaroni, *Langmuir* **2012**, *28*, 3583.

[10] E. Aznar, M. Dolores Marcos, R. Martinez-Manez, F. Sancenon, J. Soto, P. Amoros, C. Guillem, *J. Am. Chem. Soc.* **2009**, *131*, 6833.
[11] R. Martinez-Manez, F. Sancenon, M. Biyikal, M. Hecht, K. Rurack, *J. Mater. Chem.* **2011**, *21*, 12588.
[12] E. Aznar, R. Casasus, B. Garcia-Acosta, M. D. Marcos, R. Martinez-Manez, *Adv. Mater.* **2007**, *19*, 2228.
[13] N. Liu, D. R. Dunphy, P. Atanassov, S. D. Bunge, Z. Chen, G. P. López, T. J. Boyle, C. J. Brinker, *Nano Lett.* **2004**, *4*, 551.
[14] S. Angelos, Y. W. Yang, N. M. Khashab, J. F. Stoddart, J. I. Zink, *J. Am. Chem. Soc.* **2009**, *131*, 11344.
[15] B. Hille, *Ion Channels of Excitable Membranes*. Sunderland U.K. **2011**.
[16] G. J. A. A. Soler-Illia, O. Azzaroni, *Chem. Soc. Rev.* **2011**, *40*, 1107.
[17] G. J. J. A. Soler-Illia, P. Innocenzi, *Chem. Eur. J.* **2006**, *12*, 4478.
[18] R. Barbey, L. Lavanant, D. Paripovic, N. Schuewer, C. Sugnaux, S. Tugulu, H.-A. Klok, *Chem. Rev.* **2009**, *109*, 5437.
[19] R. C. Advincula, W. J. Brittain, K. C. Caster, J. Rühe, *Polymer Brushes: Synthesis Characterization, Applications*, Wiley-VCH, Weinheim, Germany **2004**.
[20] O. Azzaroni, A. A. Brown, W. T. S. Huck, *Angew. Chem. Int. Ed.* **2006**, *45*, 1770.
[21] A. Calvo, B. Yameen, F. J. Williams, G. J. A. A. Soler-Illia, O. Azzaroni, *J. Am. Chem. Soc.* **2009**, *131*, 10866.
[22] Y. Wang, F. Caruso, *Chem. Mater.* **2006**, *18*, 4089.
[23] T. D. Lazzara, K. H. A. Lau, A. I. Abou-Kandil, A.-M. Caminade, J.-P. Majoral, W. Knoll, *ACS Nano* **2010**, *4*, 3909.
[24] A. Brunsen, A. Calvo, F. J. Williams, G. J. A. A. Soler-Illia, O. Azzaroni, *Langmuir* **2011**, *27*, 4328.
[25] S. J. Minko, *J. Macromol. Sci. Polym. Rev.* **2006**, *46*, 397.
[26] B. Zhao, W. J. Brittain, *Progr. Polym. Sci.* **2000**, *25*, 677.
[27] K. Matyjaszewski, *Macromolecules* **2012**, *45*, 4015.
[28] A. S. Angelatos, Y. Wang, F. Caruso, *Langmuir* **2008**, *24*, 4224.
[29] Y. Wang, A. S. Angelatos, D. E. Dunstan, F. Caruso, *Macromolecules* **2007**, *40*, 7594.
[30] Y. Wang, F. Caruso, *Chem. Mater.* **2006**, *18*, 4089.
[31] Y. Wang, A. S. Angelatos, D. E. Dunstan, F. Caruso, *Macromolecules* **2007**, *40*, 7594.
[32] M. Kruk, B. Dufour, E. B. Celer, T. Kowalewski, M. Jaroniec, K. Matyjaszewski, *Macromolecules* **2008**, *41*, 8584.
[33] M. Kruk, *Isr. J. Chem.* **2012**, *52*, 246.
[34] R. C. Advincula, *J. Dispersion Sci. Technol.* **2003**, *24*, 343.
[35] A. Calvo, B. Yameen, F. J. Williams, O. Azzaroni, G. J. A. A. Soler-Illia, *Chem. Commun.* **2009**, 2553.
[36] R. Casasus, E. Climent, M. D. Marcos, R. Martinez-Manez, F. Sancenon, J. Soto, P. Amoros, J. Cano, E. Ruiz, *J. Am. Chem. Soc.* **2008**, *130*, 1903.
[37] M. Ali, P. Ramirez, N. Hung Quoc, S. Nasir, J. Cervera, S. Mafe, W. Ensinger, *ACS Nano* **2012**, *6*, 3631.
[38] G. Wang, A. K. Bohaty, I. Zharov, H. S. White, *J. Am. Chem. Soc.* **2006**, *128*, 13553.
[39] A. K. Bohaty, M. R. Newton, I. Zharov, *J. Porous Mater.* **2010**, *17*, 465.
[40] Y. Ma, W.-F. Dong, M. A. Hempenius, H. Mohwald, G. J. Vancso, *Nat. Mater.* **2006**, *5*, 724.
[41] M. A. Hempenius, C. Cirmi, F. Lo Savio, J. Song, G. J. Vancso, *Macromol. Rapid Commun.* **2010**, *31*, 772.
[42] E. Lallana, N. Tirelli, *Macromol. Chem. Phys.* **2013**, *214*, 143.
[43] G. R. Whittell, I. Manners, *Adv. Mater.* **2007**, *19*, 3439.
[44] I. Manners, *Synthetic Metal-Containing Polymers*, VCH: Weinheim, Germany **2004**.
[45] M. I. Giannotti, H. Lv, Y. Ma, M. P. Steenvoorden, A. R. Overweg, M. Roerdink, M. A. Hempenius, G. J. Vancso, *J. Inorg. Organomet. Polym. Mater.* **2005**, *15*, 527.
[46] M. A. Hempenius, C. Cirmi, F. Lo Savio, J. Song, G. J. Vancso, *Macromol. Rapid Commun.* **2010**, *31*, 772.
[47] A. Akhoury, L. Bromberg, T. A. Hatton, *ACS Appl. Mater. Interf.* **2011**, *3*, 1167.
[48] R. H. Staff, M. Gallei, M. Mazurowski, M. Rehahn, R. Berger, K. Landfester, D. Crespy, *ACS Nano* **2012**, *6*, 9042.
[49] J. Elbert, J. Mersini, N. Vilbrandt, C. Lederle, M. Kraska, M. Gallei, B. Stühn, H. Plenio, M. Rehahn, *Macromolecules* **2013**, *46*, 4255.
[50] J. Elbert, M. Gallei, C. Rüttiger, A. Brunsen, H. Didzoleit, B. Stühn, M. Rehahn, *Organometallics* **2013**, DOI 10.1021/om400468p.
[51] M. Mazurowski, M. Gallei, J. Y. Li, H. Didzoleit, B. Stuhn, M. Rehahn, *Macromolecules* **2012**, *45*, 8970.
[52] J. E. Spanier, I. P. Herman, *Phys. Rev. B* **2000**, *61*, 10437.
[53] D. Fattakhova-Rohlfing, M. Wark, J. Rathousky, *Chem. Mater.* **2007**, *19*, 1640.
[54] A. Walcarius, *Anal. Bioanal. Chem.* **2010**, *396*, 261.
[55] C. J. Brinker, Y. Lu, A. Sellinger, H. Fan, *Adv. Mater.* **1999**, *11*, 579.
[56] D. Grosso, F. Cagnol, G. J. A. A. Soler-Illia, E. L. Crepaldi, H. Amenitsch, A. Brunet-Bruneau, A. Bourgeois, C. Sanchez, *Adv. Funct. Mater.* **2004**, *14*, 309.
[57] M. G. Bellino, A. E. Reggazoni, G. J. A. A. Soler-Illia, *ACS Appl. Mater. Interf.* **2010**, *2*, 360.
[58] M. Etienne, A. Quach, D. Grosso, L. Nicole, C. Sanchez, A. Walcarius, *Chem. Mater.* **2007**, *19*, 844.
[59] C. J. Song, G. Villemure, *Microporous Mesoporous Mater.* **2001**, *44*, 679.
[60] A. Calvo, P. C. Anglomé, V. M. Sánchez, D. A. Scherlis, F. J. Williams, G. J. A. A. Soler-Illia, *Chem. Mater.* **2008**, *20*, 4661.
[61] A. Calvo, M. Cecilia Fuertes, B. Yameen, F. J. Williams, O. Azzaroni, G. J. A. A. Soler-Illia, *Langmuir* **2010**, *26*, 5559.
[62] M. Etienne, A. Quach, D. Grosso, L. Nicole, C. Sanchez, A. Walcarius, *Chem. Mater.* **2007**, *19*, 844.
[63] M. Etienne, Y. Guillem, D. Grosso, A. Walcarius, *Anal. Bioanal. Chem.* **2013**, *405*, 1497.
[64] G. S. Longo, M. O. de la Cruz, I. Szleifer, *Soft Matter* **2012**, *8*, 1344.
[65] D. Wang, R. J. Nap, I. Lagzi, B. Kowalczyk, S. Han, B. A. Grzybowski, I. Szleifer, *J. Am. Chem. Soc.* **2011**, *133*, 2192.
[66] L. Liu, J. B. Zhao, C. Y. Yin, P. J. Culligan, X. Chen, *Phys. Chem. Chem. Phys.* **2009**, *11*, 6520.
[67] L. Liu, J. B. Zhao, P. J. Culligan, Y. Qiao, X. Chen, *Langmuir* **2009**, *25*, 11862.
[68] A. Goux, J. Ghanbaja, A. Walcarius, *J. Mater. Sci.* **2009**, *44*, 6601.
[69] I. B. Burgess, L. Mishchenko, B. Hatton, M. Kolle, M. Loncar, J. Aizenberg, *J. Am. Chem. Soc.* **2011**, *133*, 12430.